BIOCHEMISTRY

Autoinhibited transient, gated, and cascaded dynamic transcription of RNAs

Zhenzhen Li†, Jianbang Wang†, Itamar Willner*

Following transient spatiotemporal misregulation of gene expression programs by native transcription machineries, we introduce a versatile biomimetic concept to design transient dynamic transcription machineries, revealing gated and cascaded temporal transcription of RNAs. The concept is based on the engineering of the reaction module consisting of malachite green (MG) and/or DFHBI {(5Z)-5-[(3,5-difluoro-4-hydroxyphenyl)methylene]-3,5-dihydro-2,3-dimethyl-4*H*-imidazol-4-one} DNA scaffolds, T7 RNA polymerase (RNAP) aptamer transcription scaffold, and the inhibited T7 RNAP-aptamer complex. In the presence of the counter RNAP aptamer strand and ribonucleoside triphosphates, the triggered activation of the three transcription scaffolds are activated, leading to the transcription of the MG and/or DFHBI RNA aptamer and to the transcription of the RNAP aptamer acting as an autoinhibitor that leads to the transient temporal, dissipative, and blockage of all transcription. By appropriate design of the transcription scaffolds and the inhibitors/coupler, transient gated and cascaded transcription processes are demonstrated, and a bimodal transcription module synthesizing a transient operating ribozyme is introduced.

INTRODUCTION

Transient interactions between the transcription factors or hormones and the transcription machinery play key roles in the dynamic control and modulation of gene expressions and sequestered cellular processes (*1*–*3*). Spatial and temporal misregulation between transcription factors might perturb gene expression programs, leading to a broad range of diseases (*4*). Emulating transient dynamic transcription machineries by artificial means is one of the challenges of systems chemistry (*5*–*6*), and developing these systems could provide versatile means to intervene with misregulated gene expression programs. Furthermore, dynamic branching and gene-guided expression of secondary sequestered gene expression machineries play important roles in the intercommunication of complex genetic networks and the fan-out production of multifunctional proteins (*7*–*8*). The information encoded in the base sequence of DNA (RNA) encodes substantial functional information into the biopolymer that allows the artificial engineering of complex supramolecular networks and assemblies that perform dynamic spatiotemporal modulation of transcription and gene expression machineries. Past efforts used the control over the stabilities of duplex nucleic acids and their displacement principles (*9*) and the dynamic reconfiguration of nucleic acid strands into supramolecular structures, such as G-quadruplexes (*10*, *11*), i-motif (*12*), triplexes (*13*), or aptamer-ligand complexes (*14*), by auxiliary triggers that include K^+-ion (*15*), pH (*16*), light (*17*), or sequence-specific ligands (*18*–*20*) to assemble dynamic DNA switches (*21*), DNA machines (*22*, *23*), and DNA nanostructures (*24*–*26*). These dynamic reconfigurable features of the DNA biopolymer were widely applied to develop stimuli-triggered gated nano- or micro-drug carriers (*27*, *28*), sensors (*29*, *30*), actuators (*31*), and stimuli-responsive materials, such as hydrogels (*32*, *33*). Furthermore, the base sequences comprising nucleic acids provided a means to design reconfigurable constitutional dynamic networks, revealing adaptive (*34*, *35*), hierarchically adaptive (*36*), intercommunication (*37*), and feedback-driven (*38*) properties. In particular, transient out-of-equilibrium, dissipative nucleic acid systems were reported. Enzyme-based DNA machines relying on polymerization/endonucleases/nickases were used to assemble out-of-equilibrium circuits, revealing oscillatory behaviors (*39*, *40*), gated and cascaded transient operations (*41*), or dissipative reconfiguration of constitutional dynamic networks (*42*). In addition, enzyme-guided transient release and uptake of loads and DNA ligation (*43*, *44*) and transient enzyme-driven aggregation of nanoparticles and control over their optical properties were demonstrated (*45*). All-DNA DNAzyme-driven transient systems and gated transient networks and control over transient catalytic processes were reported (*46*). Mimicking complex biological networks by artificial circuits is, however, at its infancy, and transcriptional circuits acting as transcriptional oscillators (*47*, *48*) or transcriptional switches (*49*) and bistable regulatory networks (*50*) were reported. Emulating the dynamic, transient transcription machinery–modulating gene expression is, however, still a challenge (*50*). While recent efforts addressed the triggered dynamic operation of transcriptional circuits (*51*, *52*), the out-of-equilibrium operation of transcription machineries and particularly the design of transient gated and cascaded transcriptional networks, as a means to modulate gene expression circuits (*8*), are unprecedented. In the present study, we introduce a versatile mechanism to generate transient dissipative machineries by applying a transcription machinery that transcribes the T7 RNA polymerase (RNAP) aptamer (*53*, *54*) to inhibit the RNAP. The time-dependent inhibition of RNAP leads to the transient blockage of the target transcription machinery. The time-dependent dynamic formation of the aptamer-RNAP complex yields an autoinhibitor agent for coupled transcription machineries, leading to guided transient and gated transient transcription of RNAs. In addition, by appropriate design of the transient transcription of a target RNA and its cascading to a secondary dynamic transcription machinery, the fan-out intercommunication of two autoinhibited transient modulated transcription processes is demonstrated. In addition, a bimodal autoinhibited transcription network evolving a transient operating ribozyme is introduced. Note that recent efforts were directed

The Institute of Chemistry, Center for Nanoscience and Nanotechnology, The Hebrew University of Jerusalem, Jerusalem 91904, Israel.
*Corresponding author. Email: itamar.willner@mail.huji.ac.il
†These authors contributed equally to this work.

to design intercommunicated bistable, dynamically controlled transcription machineries (*50*). In these systems, two coupled transcription networks were designed to counter-inhibit the transcription machineries to yield bistable intercommunicated transcription networks. In contrast to this approach to reaching control over dynamic transcription processes, the present study introduces a method to design transient, dissipative dynamic transcription networks by coupling two transcription machineries that lead to control over the transcription processes by an autoinhibition mechanism.

RESULTS

Transient transcription of RNA aptamers guided by autoinhibited RNAP

The application of the aptamer-RNAP autoinhibiting complex leading to the transient synthesis of RNAs is presented in Fig. 1. The reaction module is engineered to yield the transient transcription of the malachite green (MG) RNA aptamer, (**1**) (*52*). The reaction module includes two DNA templates T_1 and T_2. Template T_1 is composed of the DNA duplex composing of the scaffold (**2**) to which the promoter (**3**) and the strand (**4**) are hybridized. The scaffold (**2**) includes two domains, a and b, where domain a is complementary to the sequence a′ of (**3**) that is essential for the transcription (fig. S2) and domain b is hybridized with the domain b′ of (**4**). Note that domain a′ of strand (**3**) is extended by a toehold tether a_t'. The a_t' tether is inactive for operating the transient transcription of MG-RNA aptamer. Nonetheless, the a_t' tether will play a key role in the gated operation of the transcription machineries, vide infra. The second template T_2 consists of the scaffold (**6**) hybridized with the sequence (**7**). The scaffold (**6**) includes the domains c and d, where domain c is complementary to domain c′ of the strand (**7**) and domain d is hybridized with the domain d′ of (**7**). The ribonucleoside triphosphates (NTPs) and MG are included in the system, yet the blocked aptamer-RNAP complex eliminates any functional activity of the system. In the rest state of the module, the T7 RNAP is complexed with the RNAP aptamer (**5**) and exists at an inhibited

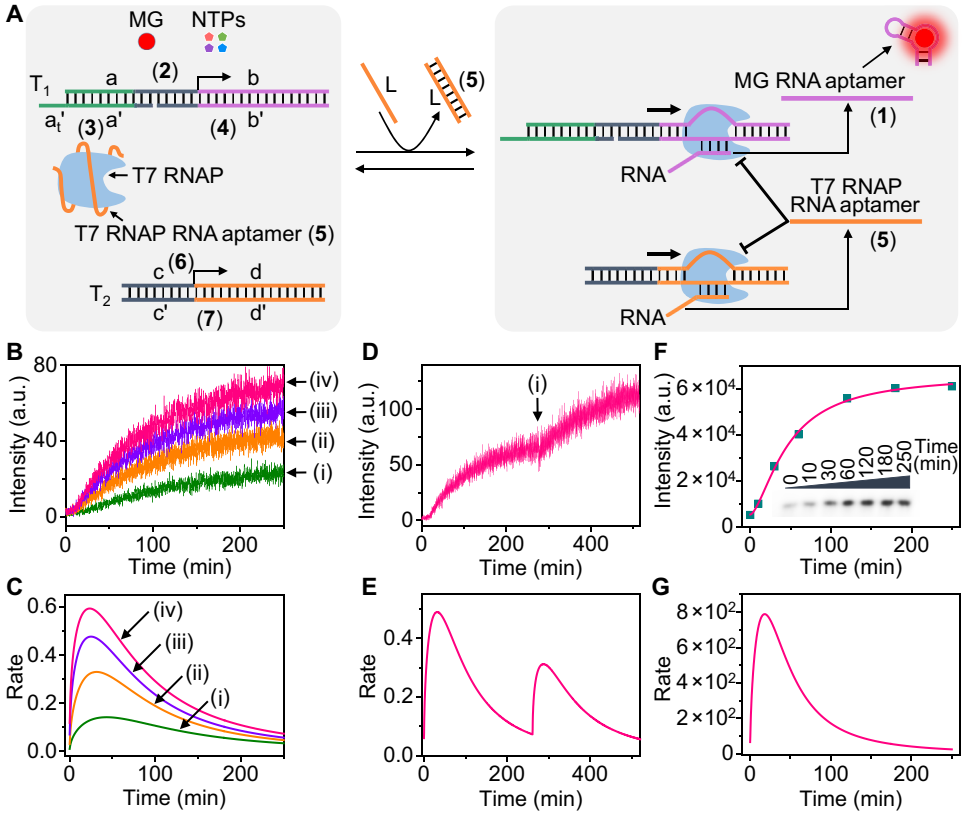

Fig. 1. Transient transcription of MG-RNA aptamer guided by autoinhibited RNAP. (**A**) Schematic triggered transient activation of the transcription of the MG-RNA aptamer through the concomitant transcription of the autoinhibiting T7 RNAP aptamer acting as control unit of the dynamic processes. (**B**) Time-dependent fluorescence changes of the MG-aptamer complex generated by the transient transcription module shown in (A) at different concentrations of the trigger L: (i) 1 μM, (ii) 2 μM, (iii) 3 μM, and (iv) 4 μM. a.u., arbitrary units. (**C**) Transient catalytic transcription rates corresponding to the MG-RNA aptamer complex formation [derivatives of the curves shown in (B)] in the presence of variable concentrations of the trigger L: (i) 1 μM, (ii) 2 μM, (iii) 3 μM, and (iv) 4 μM. (**D**) Time-dependent fluorescence changes of the MG-RNA aptamer complex upon using the transcription module shown in (A). At point (i), the trigger L (4 μM) is re-added to the rest module to activate the second cycle. (**E**) Transient catalytic transcription rates corresponding to the stepwise operation of two transcription cycles. (**F**) Probing the autoinhibited transcription module shown in (A) by an auxiliary fluorescent machinery presented in fig. S6, allowing the quantitative electrophoretic imaging of the temporal evolution of the transcribed MG-RNA aptamer. Inset: Electrophoretically separated images of the fluorescent transducing unit generated by the auxiliary fluorescent machinery. The square dots show the temporal fluorescence intensities evaluated of the temporally generated and electrophoretically separated fluorescent transducing units that follow the dynamic transcription of the MG-RNA aptamer accompanying with the fitting curve. (**G**) Rates of evolution of the fluorescent transducer units that follow the dynamics of the transcription of the MG aptamer [derivative of the fitting curve shown in (F)].

inactive configuration. The concentration of (**5**), used to completely inhibit T7 RNAP, was evaluated experimentally (see fig. S3 and accompanying discussion). Subjecting the reaction module to the "fuel" strand L that is complementary to the RNAP aptamer (**5**) results in displacing the blocking aptamer unit (**5**) to yield the L/(**5**) duplex and the activated RNAP. Unlocking of RNAP initiates, however, two competitive transcription paths, where template T_1 leads to the transcription of the MG aptamer that forms the MG-aptamer complex and template T_2 leads to the concomitant transcript of the RNAP aptamer. The later process leads to the generation of the autoinhibiting RNAP-aptamer complex. That is, the transcription of the RNAP aptamer by template T_2 leads to the dynamic self-inhibiting of RNAP and in parallel to the transient dynamic, time-dependent blockage of the transcription of the MG-aptamer driven by template T_1, ending with the switched-off initial state of the transcription process. A schematic presentation of the autoinhibited RNAP mechanism leading to the transient transcription of the MG-RNA aptamer is displayed in fig. S1. As MG in the complex state to its aptamer is fluorescent, while MG by itself is nonfluorescent, the time-dependent fluorescence changes of the MG-aptamer complex reflect the dynamics of the transcription of the MG aptamer. Figure 1B depicts the time-dependent fluorescence changes generated by the MG-aptamer complex, upon subjecting the reaction module to different concentrations of the trigger L. As the concentrations of the trigger L increase, the time-dependent fluorescence changes of the MG aptamer are intensified, consistent with the higher unlocking degree of the blocked RNAP-RNA aptamer complex to the active RNAP that guides the dissipative transcription processes. The time-dependent increase in the fluorescence intensities decrease with time, and the fluorescence intensities tend to reach saturation values, consistent with the transient blockage of the transcription processes. The time-dependent, dynamic fluorescence changes can be translated into transcription rates of the MG-RNA aptamer (derivatives of the curves shown in Fig. 1B, and these are displayed in Fig. 1C). Typical transient, dissipative transcription rates are observed, where the rate of transcription reaches a maximum value after ca. 40 min, then it depletes because of the dynamic formation of the autoinhibiting transcriptor agent (RNAP-aptamer complex), and the fully blocked transcription process is observed after ca. 200 min. The NTPs in the reaction module as substrates for the transcription process also play an important role, and the transcription of the MG aptamer is enhanced when increasing the NTP concentrations (1, 2, and 4 mM; fig. S4). The recovered "rest" reaction module that includes the templates T_1 and T_2, the blocked RNAP/aptamer structure, the free NTPs, and MG can be reactivated by the readdition of the trigger L that unlocks the dynamic transcription of the respective aptamers (Fig. 1, D and E, and fig. S5). The autoinhibited transient formation of the MG-RNA aptamer according to the scheme outlined in Fig. 1A, in the absence of the MG ligand, was independently elucidated using an auxiliary fluorescent machinery that allowed the temporal electrophoretic quantitative probing of the transcribed RNA product. The auxiliary fluorescence machinery is introduced in fig. S6 and accompanying discussion. Figure 1F (inset) depicts the temporal electrophoretically separated fluorescent bands through the hybridization between the fluorescent structure and the MG-RNA aptamer generated by the dynamic transcription machinery shown in Fig. 1A. The separated electrophoretic bands show that a time-dependent fluorescence intensity increase and the temporal increase in the contents of the aptamer were evaluated and presented in Fig. 1F. The rates of evolution of the resulting RNA (derivative of the fitting curve shown in Fig. 1F) are presented in Fig. 1G, revealing the transient formation of the respective RNA. The temporal pattern of the electrophoretically probed transient formation of the transcribed RNA fits well with the temporal assay of the fluorescent MG-aptamer complex (e.g., Fig. 1, B and C).

The design of dynamic transient transcription processes using the autoinhibiting T7 RNAP-aptamer transcription unit was further applied to design a reaction module consisting of two transcription templates, T_3 and T_2, for the triggered transient transcription of the broccoli DFHBI {(5Z)-5-[(3,5-difluoro-4-hydroxyphenyl)methylene]-3,5-dihydro-2,3-dimethyl-4*H*-imidazol-4-one} RNA aptamer (*52*). (For the detailed description of the system and the experimental results, see figs. S7 to S10.)

Gated transcription of RNA aptamers guided by autoinhibited RNAP

The successful development of a versatile scaffold to design an autoinhibited transient transcription of RNAs, exemplified with the transient transcription of the MG and DFHBI RNA aptamers, was then applied to develop gated transient transcription of target RNAs. The modulated gated transcription of a target RNA (MG or DFHBI) is addressed in Fig. 2, where the gating mechanism is referred to an auxiliary-guided selection process in the transcription of one of the aptamers (MG or DFHBI RNA aptamer). The transcription module, state I, includes three DNA templates; templates T_1 and T_3 are engineered to transcribe the MG-RNA aptamer (**1**) and DFHBI RNA aptamer (**8**), respectively; and the template T_2 is engineered to subscribe the T7 RNAP aptamer (**5**). The complex consisting of the T7 RNAP and its aptamer is included in the reaction module, leading to the inactive, inhibited structure of T7 RNAP. MG, DFHBI, and the NTP mixture are added to the reaction module. Subjecting the reaction module to the fuel strand L, complementary to the T7 RNAP aptamer (**5**), displaces the aptamer from the aptamer-T7 RNAP complex to form the energetically stabilized L/(**5**) duplex, leading to uncapping T7 RNAP to a catalytically active structure. This activates the transient dynamic system displayed in state II, where three parallel transcription processes are activated in the presence of the three templates, T_1 to T_3. The transcription proceeding on templates T_1 and T_3, yield, in parallel, the MG aptamer and the DFHBI aptamer, respectively. The transcription process proceeding on the T_2 yields, however, the T7 RNAP aptamer acting as the inhibitor of T7 RNAP. As a result, the dynamic co-synthesis of the T7 RNAP aptamer leads to the time-dependent transient inhibition of T7 RNAP and to the accompanying transient inhibition of the transcription processes proceeding on templates T_1 and T_3, resulting in the transient depletion of the transcription processes and the recovery of state I. The dynamically triggered operations of the transcription processes in state II yield the transient formation and blockage of the fluorescent MG-aptamer and DFHBI-aptamer complexes. Panel I in Fig. 3A depicts the time-dependent fluorescence changes upon the transient formation of the MG-RNA aptamer, and panel II depicts the transient rates of formation of the aptamer. Similarly, Fig. 3B (panels I and II) shows the time-dependent fluorescence changes upon transcription of the DFHBI aptamer and the transient rates corresponding to the transcription of the aptamer, respectively. Evidently, the two aptamers are generated upon triggering the reaction module in state I, and the rates of transcription of the two aptamers reveal a dissipative dynamic

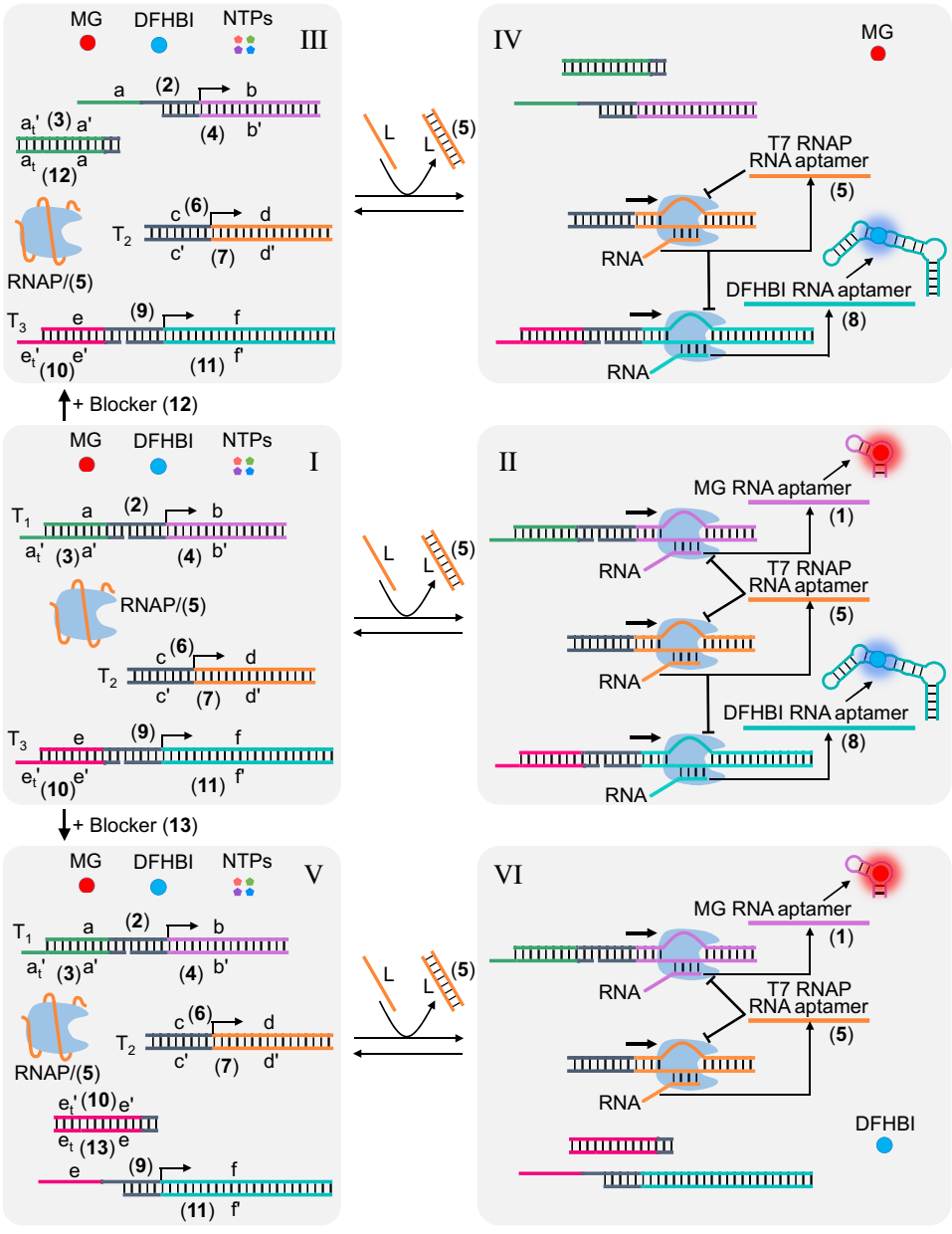

Fig. 2. Gated transcription of RNA aptamers guided by autoinhibited RNAP. Gated transient transcription of the MG-RNA aptamer and DFHBI-RNA aptamer: The module I includes three transcription scaffolds T_1 to T_3, where T_1 and T_3 act as functional scaffolds for the transcription of the MG-RNA aptamer and DFHBI-RNA aptamer, respectively, and T_2 acts as the functional template for the transcription of the T7 RNAP aptamer, acting as autoinhibitor for the dynamic transcription processes. The mute RNAP-aptamer complex is present in the rest reaction module. Subjecting the reaction module I to the trigger L leads to the formation of module II, where the parallel transient transcription of the MG-RNA aptamer and DFHBI-RNA aptamer proceeds. Treatment of module I with the blocker (**12**) inhibits the template T_1, resulting in the module in state III. Treatment of the module III with the trigger L leads to state IV, where the selective gated transient transcription of the DFHBI-RNA aptamer proceeds. Treatment of module I with the blocker (**13**) inhibits the template T_3, resulting in the module in state V. Subjecting the module V to the trigger L leads to state VI, where the selective gated transient transcription of the MG-RNA aptamer proceeds.

pattern consistent with transient inhibition of the transcription processes by the cotranscribed T7 RNAP aptamer.

Subjecting the reaction module in state I to the blocker unit (**12**) transforms state I into the reaction module in state III. The blocker (**12**) is complementary to the sequences $a_t' + a'$ of strand (**3**) being a part of template T_1. The blocker (**12**)–guided displacement of (**3**) in the form of the duplex (**12**)/(**3**) perturbs the transcription of template T_1, resulting in the templates T_2 and T_3 as the only tracks to operate the autoinhibited guided transcription reactions. Triggering state III with the fuel strand L is then anticipated to yield the intermediate state IV, where the transcription of the MG aptamer is blocked and the gated transient transcription of the DFHBI aptamer proceeds. The gating efficiency is, however, expected to be controlled by the concentration of the blocker unit (**12**). As the concentration

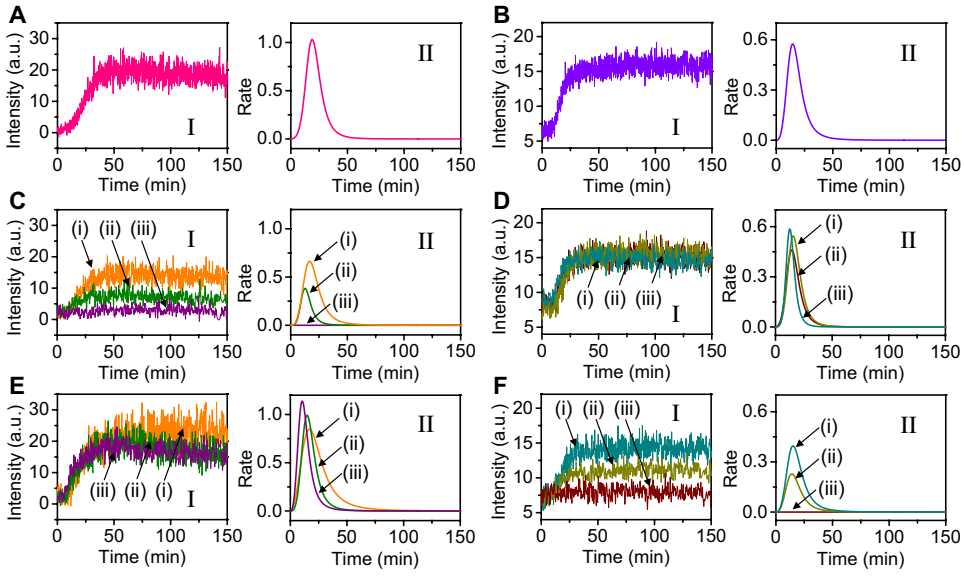

Fig. 3. Dynamic fluorescence changes transduced by the autoinhibited RNAP-stimulated transcription of MG/DFHBI aptamers. Nongated transient transcription of (**A**) the MG-RNA aptamer: panel I, time-dependent fluorescence changes of the MG-aptamer complex; panel II, transient catalytic rates corresponding to the formation of the MG-RNA aptamer. (**B**) The DFHBI-RNA aptamer: panel I, time-dependent fluorescence changes of the DFHBI-aptamer complex; panel II, transient catalytic rates corresponding to the formation of the DFHBI-RNA aptamer. Gated transcription of the MG-RNA or DFHBI-RNA aptamer in the presence of the inhibitor (**12**) or (**13**): (**C**) Panel I, time-dependent fluorescence changes of the MG-aptamer complex in the presence of variable concentrations of inhibitor (**12**): (i) 2.5 nM, (ii) 5 nM, and (iii) 50 nM; panel II, transient catalytic rates for the transient transcription of the MG aptamer in the presence of the respective concentrations of (**12**). (**D**) Panel I, time-dependent fluorescence changes of the DFHBI-aptamer complex in the presence of variable concentrations of inhibitor (**12**): (i) 2.5 nM, (ii) 5 nM, and (iii) 50 nM; panel II, transient catalytic rates for the transient transcription of the DFHBI aptamer in the presence of the respective concentrations of (**12**). (**E**) Panel I, time-dependent fluorescence changes of the MG-aptamer complex in the presence of variable concentrations of inhibitor (**13**): (i) 5 nM, (ii) 10 nM, and (iii) 100 nM; panel II, transient catalytic rates for the transient transcription of the MG aptamer in the presence of the respective concentrations of (**13**). (**F**) Panel I, time-dependent fluorescence changes of the DFHBI-aptamer complex in the presence of variable concentrations of inhibitor (**13**): (i) 5 nM, (ii) 10 nM, and (iii) 100 nM; panel II, transient catalytic rates for the transient transcription of the DFHBI aptamer in the presence of the respective concentrations of (**13**).

of (**12**) is elevated, the selectivity of the gated transcription is enhanced. Figure 3C (panel I) depicts the time-dependent fluorescence changes of the MG-aptamer complex observed in the presence of variable concentrations of (**12**). As the concentration of (**12**) is elevated, the fluorescence generated by the MG-aptamer complex is lowered, and at a concentration of (**12**) = 50 nM, no fluorescence of the MG-aptamer complex is observed (Fig. 3C, panel I, curve iii). At this concentration, the transcription of the MG aptamer is fully switched off (Fig. 3C, panel II, curve iii). In turn, the addition of blocker (**12**) has no effect on the time-dependent fluorescence changes of the DFHBI-aptamer complex (Fig. 3D, panel I) or on the dissipative transient transcription rates of DFHBI aptamer (Fig. 3D, panel II). Treatment of the reaction module in state I with the blocker unit (**13**) leads to the gated transcription of the MG-RNA aptamer, state V. The blocker (**13**) displaces the strand (**10**) associated with template T_3 to yield the energetically stabilized duplex (**10**)/(**13**), resulting in the perturbation and blockage of the transcription of DFHBI aptamer on template T_3. In the presence of the trigger L, the transcription of the T_1 and T_2 templates is activated, leading to the gated transient transcription of the MG aptamer. Figure 3E shows the time-dependent fluorescence changes of the MG-aptamer complex resulting upon the blocker (**13**)–controlled operation of state V in the presence of variable concentrations of (**13**). The formation of the MG aptamer is not affected by blocker (**13**) and shows a dissipative kinetic rate profile (Fig. 3E, panel II). In turn, the blocker (**13**) inhibits the formation of the DFHBI aptamer (Fig. 3F, panels I and II). At a concentration of (**13**) = 100 nM, the formation of the DFHBI aptamer is fully blocked (Fig. 3F, curve iii in panels I and II), consistent with the selective gated dynamic formation of the MG aptamer that reveals the dynamic dissipative rate profile. That is, the gating degree is controlled by the concentration of the respective blocker unit added to the reaction module. As the concentration of the blocker unit is elevated, the inhibition of the respective transcription template is enhanced, resulting in a higher degree of gating.

Temporal cascaded autoinhibited RNAP-driven transcription of MG/DFHBI aptamers

In the next step and inspired by nature where operation of intercommunicated transcriptional cascades plays important roles in gene expressions, we applied the "suicide" transcriptor vehicle to design a transient cascaded transcriptional machinery as outlined in Fig. 4. The rest module of the system, state M includes the duplex template T_4 consisting of the scaffold (**14**) hybridized with the promoter (**3**) and the strand (**15**); the duplex of the scaffold (**9**) hybridized with the strand (**11**); the duplex nucleic acid (**16**)/(**17**), acting as intercommunicating unit to activate the transcriptional cascade; the duplex (**6**)/(**7**), acting as the template for the T7 RNAP inhibiting aptamer; and the aptamer (**5**)–blocked T7 RNAP biocatalyst, as constituent that drives the cascaded transcriptional machinery. MG, DFHBI, and the NTPs are added to the module as auxiliary components. The constituent (**14**)/(**3**)/(**15**) is engineered to include in the subdomains a + b/a_t' + a′ + b′, the functional sequences to drive the transcription of the MG-RNA aptamer. The scaffold (**14**) includes the domains e′ + e_x', and the strand (**15**) contains the

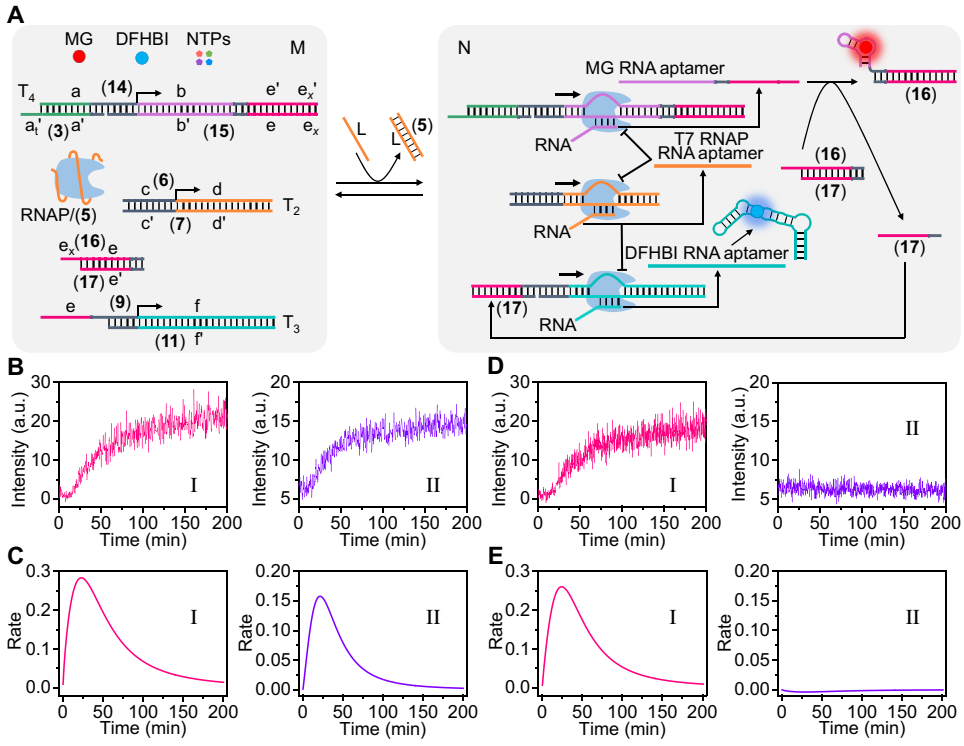

Fig. 4. Transient temporal cascaded transcription of MG/DFHBI aptamers driven by the autoinhibited RNAP. (**A**) Transient cascaded transcription of the MG-RNA aptamer and DFHBI-RNA aptamer guided by the autoinhibited T7 RNAP. The reaction module consists of the transcription scaffolds T_4, T_2, and T_3; the mute inactivated RNAP/aptamer (**5**) complex; and the coupling duplex (**16**)/(**17**). The L-triggered activation of RNAP stimulates the transcription of the MG-RNA aptamer that includes the tether e′ + e_x′, and the tether displaces the duplex (**16**)/(**17**) to release the promoter (**17**) that activates the transcription of the DFHBI-RNA aptamer using DNA template T_3. Concomitantly, the transcription of the RNAP aptamer by template T_2 yields the inhibiting aptamer that leads to the dissipative blockage of all transcription processes in the system. (**B**) Time-dependent fluorescence changes associated with panel I, the transcription of the MG-RNA aptamer, and panel II, the cascaded transcription of the DFHBI-RNA aptamer. (**C**) Transient catalytic rates corresponding to panel I, the transcription of the MG-RNA aptamer, and panel II, the cascaded transcription of the DFHBI-RNA aptamer. (**D** and **E**) Control experiment demonstrating the operation of the reaction module M upon exclusion of the duplex (**16**)/(**17**). (D) Panel I, time-dependent fluorescence changes upon transcription of the MG-RNA aptamer; panel II, fully inhibited fluorescence of the DFHBI-RNA aptamer complex. (E) Catalytic rates corresponding to the blocked catalytic cascade: panel I, transient, dissipative rates corresponding to the formation of the MG-RNA aptamer; panel II, fully blocked catalytic rates for the formation of the DFHBI aptamer.

domains e and e_x. As a result, the transcribed MG-RNA aptamer by the constituent (**14**)/(**3**)/(**15**) includes an RNA tether composed the complementary ribonucleobases to e + e_x. This tether acts as the signal promoter to couple the MG aptamer transcription with the DFHBI aptamer transcription machinery. The tether e + e_x associated with the coupler duplex (**16**)/(**17**) to yield the free strand (**17**) that hybridizes as promoter to the constituent (**9**)/(**11**) to yield the intact DFHBI aptamer transcription scaffold. The module in state M exists in a mute inactive configuration. Subjecting, however, the system to trigger L [counter strand to the T7 RNAP inhibiting aptamer (**5**)] activates the transient, dissipative, cascaded transcription processes, state N. The triggered displacement of the inhibiting aptamer (**5**) activates the T7 RNAP that stimulates the activation of the transcription process using the (**14**)/(**3**)/(**15**) template that results in the transcription of the MG-RNA aptamer with a tether. The later transcribed aptamer displaces the coupler unit (**16**)/(**17**) that leads to the formation of the template (**9**)/(**17**)/(**11**) that acts as template for the transcription of the DFHBI-RNA aptamer. Concomitantly to the transcription of the MG-RNA and DFHBI-RNA aptamers, the template (**6**)/(**7**) is activated toward the transcription of the T7 RNAP aptamer that results in the competitive inhibition of RNAP, leading to the transient inhibition of all transcription processes (the cascaded transcription of the MG and DFHBI aptamer and the transcription of the T7 RNAP aptamer itself). As a result, the entire dynamic transcription system undergoes dissipative depletion that regenerates the rest module in state M. The transient dynamic transcription of the MG-RNA aptamer and the DFHBI-RNA aptamer is then followed by the transient fluorescence features of the resulting MG-aptamer and DFHBI-aptamer complexes. Figure 4B (panels I and II) shows the time-dependent fluorescence changes of the resulting MG-aptamer and DFHBI-aptamer complexes, respectively. Figure 4C (panels I and II) shows the transcription rates corresponding to the formation of the MG aptamer and the DFHBI aptamer, respectively, by the cascaded transcription machinery (derivatives of the curves displayed in Fig. 4B, panels I and II). The transcription rates reveal, as expected, a transient, dissipative pattern. Figure 4D depicts the results of a control experiment, where the coupling duplex (**16**)/(**17**) is excluded from the transcription module consisting of the (**14**)/(**3**)/(**15**), (**9**)/(**11**), (**6**)/(**7**), and the blocked T7 RNAP-aptamer complex unit; and the module is subjected to the trigger L in the presence of MG, DFHBI, and NTPs as additional components. Under these conditions, the transcription cascade is blocked, and only the dynamic transient transcription of the MG-RNA aptamer proceeds (Fig. 4, D and E, panels I and II, respectively).

Temporal transcription of transient ribozymes by the autoinhibited RNAP

Beyond the transient dynamic rate profiles of the transcription and gated transcription of the MG and DFHBI aptamers using the transcription of the T7 RNAP aptamer, we applied the autoinhibited RNAP-aptamer complex to demonstrate the dissipative transcription of a ribozyme revealing transient catalytic functions (Fig. 5). The reaction module (Fig. 5A) includes the transcription template T_5 composed of the strands (**18**)/(**3**)/(**19**), the transcription template T_2, (**6**)/(**7**), that transcribes the inhibiting T7 RNAP aptamer, and the transcription template T_6 composed of the strands (**20**)/(**10**)/(**21**). The substrate (**22**) modified by the fluorophore/quencher pair ROX (carboxy-X-rhodamine)/BHQ2 (Black Hole Quencher-2), the aptamer-blocked T7 RNAP, and the NTP mixture are also included in the reaction module. Triggering of the reaction module with the fuel strand L displaces the blocking aptamer bound to T7 RNAP, resulting in its uncapping and the activation of the three transcription processes associated with the templates T_5, T_2, and T_6. The transcription processes proceeding on templates T_5 and T_6 yield the ribozymes **1** and **2**, respectively, while the transcription occurring on the template T_2 generates the autoinhibiting T7 RNAP aptamer unit that inhibits the transcription biocatalyst. The transcribed ribozyme **1** was designed to cleave substrate (**22**) and concomitantly to be cleaved by ribozyme **2**, resulting in the temporal depletion of ribozyme **1** and the accompanying blockage of cleavage of substrate (**22**). The transcription processes proceeding on the three transcription templates lead to a dynamically controlled transcription of the ribozymes, where the time-dependent emergence of the T7 RNAP aptamer leads to a transient blockage of the formation of the ribozymes and the catalytic functions. The formation and depletion of the transcribed ribozyme **1** are followed by probing the time-dependent fluorescence changes originating from the ribozyme **1**–guided cleavage of the substrate (**22**). Figure 5B depicts the time-dependent fluorescence changes of the fragmented substrate (**22**), reflecting the dynamic transient activity of the ribozyme **1** cleaving the substrate (**22**). Figure 5C shows the time-dependent catalytic rate of the transcribed ribozyme **1** (derivative of the time-dependent fluorescence curve shown in Fig. 5B). A characteristic dissipative dynamic kinetic profile corresponding to the catalytic activity of the resulting ribozyme is observed. The transient temporal activity of ribozyme **1** was further supported by electrophoretic measurement that quantitatively follows the fluorescence of the temporal formation and blockage of the electrophoretically separated ROX-labeled product. Figure 5D (inset) shows the electrophoretic bands of samples of the electrophoretically separated ROX-labeled fragment withdrawn from the reaction system at time intervals of transcriptional evolution of ribozyme **1**. The temporal fluorescence intensities of the ROX-labeled strand are displayed as square dots in Fig. 5D accompanying with the fitting curve. The transient fluorescence intensities of the ROX-labeled strand follow the dynamic catalytic rates of ribozyme **1**. Accordingly, Fig. 5E depicts the derivative of the curve displayed in Fig. 5D. The transient catalytic behavior of ribozyme **1** traced by the dynamic contents of the ROX-labeled fragment from the electrophoretic bands is consistent to that derived from the cleavage rates of (**22**) shown in Fig. 5C.

DISCUSSION

The recent study has introduced a versatile mechanism to modulate the transient operation of the transcription machineries by the dynamic control of the transient formation of the autoinhibited T7

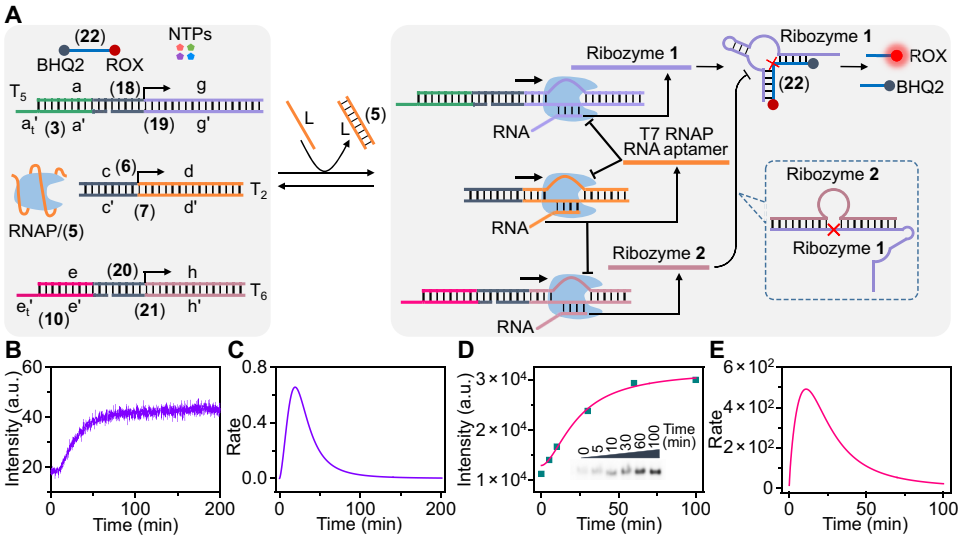

Fig. 5. Temporal transcription of transient ribozymes by the autoinhibited RNAP. (**A**) Schematic assembly of a bimodal autoinhibited transient transcription network generating two intercommunicating ribozymes that yield a transient operating ribozyme **1**. The temporal operation of ribozyme **1** is followed by the temporal cleavage of the ROX/BHQ2 modified substrate (**22**). (**B**) Temporal fluorescence changes of the fragmented substrate generated by the transient ribozyme **1** upon cleavage of its substrate (**22**). (**C**) Rate of temporal transient operation of ribozyme **1** upon cleavage of its substrate (**22**) [derivative of the curve depicted in (B)]. (**D**) Probing the autoinhibited transcription module shown in (A) by the quantitative electrophoretic imaging of the temporal evolution of the transcribed ribozyme **1**. Inset: Electrophoretically separated images of the fragmented substrate (**22**) generated through the cleavage by the ribozyme **1**. The square dots show the temporal fluorescence intensities evaluated of the temporally generated and electrophoretically separated fluorescent units that follow the dynamic transcription and depletion of the ribozyme **1** accompanying with the fitting curve. (**E**) Rates of evolution of the fluorescent units that follows the dynamics of the transcription and depletion of the ribozyme **1** [derivative of the curve shown in (D)].

RNAP. The study demonstrated the application of the dynamically modulated transcription processes for the synthesis of different RNA aptamers, stimulated gated transcription processes and transient dissipative, cascaded transcription processes, and the synthesis of ribozymes that demonstrates temporal catalytic functions. Beyond providing artificial means to emulate natural dynamically modulated gene expression processes, the study might introduce important paths for therapeutic applications. The dynamic temporal modulation of gene expression and translated proteins could provide versatile means for the biomarker-triggered dose release of therapeutic agents (*55*–*57*). Nonetheless, important challenges are ahead of us: The integration of the dynamically modulated transcription machineries into protocell carriers (*58*, *59*) and the coupling of the transient transcription mechanisms to dynamic protein translation paths are important paths to follow.

MATERIALS AND METHODS

Materials

T7 RNAP (50,000 U ml^{-1}, 0.81 μM), RNAP reaction buffer, and ribonucleotide solution mix [rATP (rAdenosine triphosphate), rCTP (rCytidine triphosphate), rGTP (rGuanosine triphosphate), and rUTP (rUridine triphosphate)] were purchased from New England Biolabs Inc. MG and DFHBI were purchased from Sigma-Aldrich. Oligonucleotides were purchased from Integrated DNA Technologies and Sigma-Aldrich. All the sequences of the oligonucleotides were listed as follows: (**2**), 5′-ATTGAGGTAAGAAAGGTAAGGATAATACGACTCAC-TATAGGATCCCGACTGGCGAGAGCCAGGTAACGAATGGATCC-3′; (**3**), 5′-TATTATCCTTACCTTTCTTACCTCAATCTCCTTCG-3′; (**4**), 5′-GGATCCATTCGTTACCTGGCTCTCGCCAGTCGGGATC-CTATAGTGAGTCG-3′; (**5**), 5′-rGrGrCrGrArGrCrGrUrArArGrUr-CrArArUrUrCrCrArCrUrArUrCrArUrUrGrCrUrGrCrArArGrC-3′; (**6**), 5′-AGCTTAATACGACTCACTATAGGCGAGCGTAAGTCAAT-TCCACTATCATTGCTGCAAGC-3′; (**7**), 5′-GCTTGCAGCAATGATAGT-GGAATTGACTTACGCTCGCCTATAGTGAGTCGTATTAAGCT-3′; (**9**), 5′-CTAATGAACTACTACTACACACTAATACGACT-CACTATAGGAACGAGACGGTCGGGTCCAGATATTCG-TATCTGTCGAGTAGAGTGTGGGCTCGTTCC-3′; (**10**), 5′-TATTAGTGTGTAGTAGTAGTTCATTAGTGTCCATG-3′; (**11**), 5′-GGAACGAGCCCACACTCTACTCGACAGATACGAA-TATCTGGACCCGACCGTCTCGTTCCTATAGTGAGTCG-3′; (**12**), 5′-CGAAGGAGATTGAGGTAAGAAAGGTAAGGATAATA-3′; (**13**), 5′-CATGGACACTAATGAACTACTACTACA-CACTAATA-3′; (**14**), 5′-ATTGAGGTAAGAAAGGTA-AGGATAATACGACTCACTATAGGATCCCGACTGGC-GAGAGCCAGGTAACGAATGGATCCTTTTTTATT-AGTGTGTAGTAGTAGTTCATTAGGGTTCATG-3′; (**15**), 5′-CATGAACCCTAATGAACTACTACTACACACTAATAA AAAGGATCCATTCGTTACCTGGCTCTCGCCAGTC-GGGATCCTATAGTGAGTCG-3′; (**16**), 5′-CATGAAC-CCTAATGAACTACTACTACACACTAATA-3′; (**17**), 5′-TATTAGTGTGTAGTAGTAGTTCATTAG-3′; (**18**), 5′-ATTGAGG-TAAGAAAGGTAAGGATAATACGACTCACTATAGGTAC-GAGTCCTCCCTGATGAGGCCGAAAGGCCGAAATCCTGA-3′; (**19**), 5′-TCAGGATTTCGGCCTTTCGGCCTCATCAGGGAG-GACTCGTACCTATAGTGAGTCG-3′; (**20**), 5′-CTAATGAAC-TACTACTACACACTAATACGACTCACTATAGGCCT-CATCAGGCTGATGAGCGAAAGGACTCGTACC-3′; (**21**), 5′-GGTACGAGTCCTTTCGCTCATCAGCCTGATGAGGCC TATAGTGAGTCG-3′, (**22**) 5′-ROX-TCAGGATrAGGAGGAC-BHQ2-3′; (**23**), 5′-TGTCTACAGTGCGTGCTCCTCGACTGGCGAGAGC-CAGGTAAC-3′; (**24**) 5′-GGATCCATTCGTTACCTGGCTCTC-GCCAGTCGCCGTCAAGACCCAGCAAC-3′; (**25**), 5′-Cy3-AGGAGCACGCACTGTAGACA-3′; (**26**), 5′-GTTGCTG-GGTCTTGACGG-BHQ2-3′; (**27**), 5′-ACAAACAGATGC-GTGCTCCTCGTATCTGTCGAGTAGAGTGTG-3′; (**28**), 5′-GGAACGAGCCCACACTCTACTCGACAGATACGC-CGTCAAGACCCAGCAAC-3′; (**29**), 5′-Cy5-AGGAGCACG-CATCTGTTTGT-3′

Characterizations

All the fluorescence spectra were recorded with a Cary Eclipse Fluorescence Spectrophotometer (Varian Inc.) at 37°C using the quartz cuvette (Hellma Analytics). The excitation and emission of the MG-RNA aptamer complex, DFHBI-RNA aptamer complex, and the ROX were performed at 635/665, 470/500, and 588/608 nm, respectively. The polyacrylamide gel electrophoresis (PAGE) gels were run on a Hoefer SE 600 electrophoresis unit (10 or 20%, 80 V, at 4°C), and the images of the gels were recorded on the ChemiDoc MP Imaging System and analyzed using the ImageJ software.

Methods

Dynamic transcription of the MG aptamer

The transient reaction module for the transcription of the MG aptamer was a mixture of the DNA templates T_1 (**2**)/(**3**)/(**4**) (0.01 μM) and T_2 (**6**)/(**7**) (0.05 μM); the prepared inhibited T7 RNAP-aptamer complex that composed of the T7 RNAP, 0.06 μM mixing with the inhibiting aptamer (**5**), 2 μM, for a time interval of 60 min to ensure full inhibition of the T7 RNAP; and MG (2 μM) and the NTPs (4 mM each) in the RNAP reaction buffer [40 mM tris-HCl, 1 mM dithiothreitol (DTT), 2 mM spermidine, and 20 mM $MgCl_2$ (pH 7.9)]. Variable concentrations of the fuel strand L (1 to 4 μM) were applied to the reaction module, and the dynamic time-dependent fluorescence changes of the MG-aptamer complex were recorded with a Cary Eclipse Fluorescence Spectrophotometer (Varian Inc.) at λ_{em} = 665 nm (37°C).

For the control experiment, the strand (**3**) was excluded from the reaction module. The constituents of the reaction module included the (**2**)/(**4**) (0.01 μM) and (**6**)/(**7**) (0.05 μM); the prepared inhibited T7 RNAP-aptamer complex that composed of the T7 RNAP, 0.06 μM mixing with the inhibiting aptamer (**5**), 2 μM, for a time interval of 60 min to ensure full inhibition of the T7 RNAP; and MG (2 μM) and the NTPs (4 mM each) in the RNAP reaction buffer [40 mM tris-HCl, 1 mM DTT, 2 mM spermidine, and 20 mM $MgCl_2$ (pH 7.9)]. A concentration of 4 μM of the fuel strand L was applied to the reaction module, and the time-dependent fluorescence changes were recorded with a Cary Eclipse Fluorescence Spectrophotometer (Varian Inc.) at λ_{em} = 665 nm (37°C).

For the measurement of the dynamic transcription of the MG aptamer at variable concentrations of NTPs, three reaction module samples were prepared including the same concentrations of T_1 (**2**)/(**3**)/(**4**) (0.01 μM), T_2 (**6**)/(**7**) (0.05 μM), the prepared inhibited T7 RNAP-aptamer complex and MG (2 μM), and different concentrations of the NTPs (1, 2, and 4 mM each, respectively). All the three samples were applied with the same concentrations of the fuel strand L (2 μM), and the time-dependent fluorescence changes were recorded with a Cary Eclipse Fluorescence Spectrophotometer (Varian Inc.) at λ_{em} = 665 nm (37°C).

For the cyclic transient transcription of the MG aptamer, the reaction module was applied twice with the fuel strand L: 4 and 4 or 2 and 4 μM, respectively. The dynamic time-dependent fluorescence changes of the MG-aptamer complex were recorded with a Cary Eclipse Fluorescence Spectrophotometer (Varian Inc.) at λ_{em} = 665 nm (37°C).

For the PAGE measurement, a volume of 10 μl was collected from the reaction solution [0.01 μM T_1 (**2**)/(**3**)/(**4**), 0.05 μM T_2 (**6**)/(**7**), 0.06 μM inhibited T7 RNAP, 4 mM NTPs, and 4 μM fuel strand L] at different time intervals (0, 10, 30, 60, 120, 180, and 250 min). Then, they were mixed with the Y-shaped quenched fluorophore structure (**23**)/(**24**)/(**25**)/(**26**) (0.5 μM) and annealed from 70° to 4°C. All the samples were loaded into the 10% PAGE gel to perform at 80 V for 12 hours (4°C). The image of the gel was recorded on the ChemiDoc MP Imaging System and analyzed using the ImageJ software.

Dynamic transcription of the DFHBI aptamer

The transient reaction module for the transcription of the DFHBI aptamer was a mixture of the DNA templates T_3 (**9**)/(**10**)/(**11**) (0.02 μM) and T_2 (**6**)/(**7**) (0.1 μM); the prepared inhibited T7 RNAP-aptamer complex that composed of the T7 RNAP, 0.12 μM mixing with the inhibiting aptamer (**5**), 4 μM, for a time interval of 60 min to ensure full inhibition of the T7 RNAP; and DFHBI (4 μM) and the NTPs (4 mM each) in the RNAP reaction buffer [40 mM tris-HCl, 1 mM DTT, 2 mM spermidine, and 20 mM $MgCl_2$ (pH 7.9)]. Variable concentrations of the fuel strand L (2, 4, 6, and 8 μM) were applied to the reaction module, and the dynamic time-dependent fluorescence changes of the DFHBI-aptamer complex were recorded with a Cary Eclipse Fluorescence Spectrophotometer (Varian Inc.) at λ_{em} = 500 nm (37°C).

For the cyclic transient transcription of the DFHBI aptamer, the reaction module was applied twice with the fuel strand L: 6 and 6 μM, respectively. The dynamic time-dependent fluorescence changes of the DFHBI-aptamer complex were recorded with a Cary Eclipse Fluorescence Spectrophotometer (Varian Inc.) at λ_{em} = 500 nm (37°C).

For the PAGE measurement, a volume of 10 μl was collected from the reaction solution [0.02 μM T_1 (**9**)/(**10**)/(**11**), 0.1 μM T_2 (**6**)/(**7**), 0.12 μM inhibited T7 RNAP, 4 mM NTPs, and 8 μM fuel strand L] at different time intervals (0, 5, 10, 20, 40, 90, and 150 min). Then, they were mixed with the Y-shaped quenched fluorophore structure (**27**)/(**28**)/(**29**)/(**26**) (1 μM) and annealed from 70° to 4°C. All the samples were loaded into the 10% PAGE gel to perform at 80 V for 12 hours (4°C). The image of the gel was recorded on a ChemiDoc MP Imaging System and analyzed using the ImageJ software.

Transient gated operations of the transcription processes

The composition of the reaction module I included three DNA templates, T_1 (0.005 μM), T_2 (0.075 μM), and T_3 (0.01 μM), and the RNAP/(**5**)–caged catalyst. MG (2 μM), DFHBI (4 μM), and NTPs (4 μM each) were included in the system. The T7 RNAP (0.09 μM) was mixed with the inhibiting aptamer (**5**) (3 μM) for a time interval of 60 min to ensure full inhibition of T7 RNAP. The DNA templates T_1 to T_3 were then added to the inhibited RNAP/(**5**) complex, and MG, DFHBI, and the NTPs were added to the mixture in the RNAP reaction buffer [40 mM tris-HCl, 1 mM DTT, 2 mM spermidine, and 20 mM $MgCl_2$ (pH 7.9)]. The transient dynamic transcription of the templates was triggered by adding the fuel strand L (8 μM). The dynamic transcription of the MG and DFHBI aptamers were followed by the time-dependent fluorescence changes of the MG/aptamer complex at λ_{em} = 665 nm and of the DFHBI/aptamer complex at λ_{em} = 500 nm, recording with a Cary Eclipse Fluorescence Spectrophotometer (Varian Inc.) at 37°C.

To gate the respective transcription processes, the reaction module I was subjected to variable concentrations of the inhibitor (**12**) (2.5, 5, and 50 nM) or (**13**) (5, 10, and 100 nM), for a time interval of 10 min, and the respective dynamic transcription processes were triggered by L (8 μM), followed by monitoring the time-dependent fluorescence changes of the respective RNA-aptamer ligand complexes using a Cary Eclipse Fluorescence Spectrophotometer (Varian Inc.) at 37°C.

Transient cascaded transcription processes

The transient cascaded reaction module M included the DNA templates T_4 (**14**)/(**3**)/(**15**) (0.005 μM), T_2 (**6**)/(**7**) (0.075 μM), and T_3 (**9**)/(**11**) (0.01 μM); the coupling duplex (**16**)/(**17**) (0.02 μM); and the prepared inhibited T7 RNAP/aptamer complex that composed of the T7 RNAP, 0.09 μM mixing with the inhibiting aptamer (**5**), 3 μM, for a time interval of 60 min to ensure full inhibition of T7 RNAP; and MG (2 μM), DFHBI (4 μM), and the NTPs (4 mM each) in the RNAP reaction buffer [40 mM tris-HCl, 1 mM DTT, 2 mM spermidine, and 20 mM $MgCl_2$ (pH 7.9)]. The dissipative dynamic cascaded transcription of the MG aptamer and the DFHBI aptamer were activated by adding the fuel strand L (8 μM), and the time-dependent fluorescence changes of the MG-aptamer complex and DFHBI-aptamer complex were recorded with a Cary Eclipse Fluorescence Spectrophotometer (Varian Inc.) at λ_{em} = 665 and 500 nm, respectively (37°C).

For the control experiment, the coupling duplex (**16**)/(**17**) was excluded from the reaction module M, and the other components were the same as before including the DNA templates T_4 (**14**)/(**3**)/(**15**) (0.005 μM), T_2 (**6**)/(**7**) (0.075 μM), and T_3 (**9**)/(**11**) (0.01 μM); the prepared inhibited T7 RNAP/aptamer complex; and MG (2 μM), DFHBI (4 μM), and the NTPs (4 mM each). The dynamic transcription of the MG aptamer and the DFHBI aptamer were activated by adding the fuel strand L (8 μM), and the time-dependent fluorescence changes of the MG-aptamer complex and DFHBI-aptamer complex were recorded with a Cary Eclipse Fluorescence Spectrophotometer (Varian Inc.) at λ_{em} = 665 and 500 nm, respectively (37°C).

Temporal transcription of transient ribozymes

The transient reaction module for the transcription of the transient ribozymes was a mixture of the DNA templates T_5 (**18**)/(**3**)/(**19**) (0.01 μM), T_2 (**6**)/(**7**) (0.05 μM), and T_6 (**20**)/(**10**)/(**21**) (0.01 μM); the prepared inhibited T7 RNAP/aptamer complex that composed of the T7 RNAP, 0.07 μM mixing with the inhibiting aptamer (**5**), 2.4 μM, for a time interval of 60 min to ensure full inhibition of the T7 RNAP; and the substrate (**22**) (2 μM) and the NTPs (4 mM each) in the RNAP reaction buffer [40 mM tris-HCl, 1 mM DTT, 2 mM spermidine, and 20 mM $MgCl_2$ (pH 7.9)]. The fuel strand L (8 μM) was applied to the reaction module, and the dynamic time-dependent fluorescence changes of the fragmented (**22**) were recorded with a Cary Eclipse Fluorescence Spectrophotometer (Varian Inc.) at λ_{em} = 608 nm (37°C).

For the PAGE measurement, a volume of 10 μl was collected from the reaction solution at different time intervals (0, 5, 10, 30, 60, and 100 min), and they were loaded into the 20% PAGE gel to perform at 80 V for 20 hours (4°C). The image of the gel was recorded on a ChemiDoc MP Imaging System and analyzed using the ImageJ software.

SUPPLEMENTARY MATERIALS

Supplementary material for this article is available at https://science.org/doi/10.1126/sciadv.abq5947

View/request a protocol for this paper from *Bio-protocol*.

REFERENCES AND NOTES

1. T. L. Lenstra, J. Rodriguez, H. Chen, D. R. Larson, Transcription dynamics in living cells. *Annu. Rev. Biophys.* **45**, 25–47 (2016).
2. G. L. Hager, J. G. McNally, T. Misteli, Transcription dynamics. *Mol. Cell* **35**, 741–753 (2009).
3. C. M. Weber, S. Henikoff, Histone variants: Dynamic punctuation in transcription. *Genes Dev.* **28**, 672–682 (2014).
4. T. I. Lee, R. A. Young, Transcriptional regulation and its misregulation in disease. *Cell* **152**, 1237–1251 (2013).
5. R. F. Ludlow, S. Otto, Systems chemistry. *Chem. Soc. Rev.* **37**, 101–108 (2008).
6. G. Ashkenasy, T. M. Hermans, S. Otto, A. F. Taylor, Systems chemistry. *Chem. Soc. Rev.* **46**, 2543–2554 (2017).
7. X. Guo, F. Li, L. Bai, W. Yu, X. Zhang, Y. Zhu, D. Yang, Gene circuit compartment on nanointerface facilitatating cascade gene expression. *J. Am. Chem. Soc.* **141**, 19171–19177 (2019).
8. V. M. Weake, J. L. Workman, Inducible gene expression: Diverse regulatory mechanisms. *Nat. Rev. Genet.* **11**, 426–437 (2010).
9. F. C. Simmel, B. Yurke, H. R. Singh, Principles and applications of nucleic acid strand displacement reactions. *Chem. Rev.* **119**, 6326–6369 (2019).
10. H. Yang, Y. Zhou, J. Liu, G-quadruplex DNA for construction of biosensors. *Trends Anal. Chem.* **132**, 116060 (2020).
11. D.-L. Ma, Z. Zhang, M. Wang, L. Lu, H.-J. Zhong, C.-H. Leung, Recent developments in G-quadruplex probes. *Chem. Biol.* **22**, 812–828 (2015).
12. Y. Dong, Z. Yang, D. Liu, DNA nanotechnology based on i-motif structures. *Acc. Chem. Res.* **47**, 1853–1860 (2014).
13. Y. Hu, A. Cecconello, A. Idili, F. Ricci, I. Willner, Triplex DNA nanostructures: From basic properties to applications. *Angew. Chem. Int. Ed.* **56**, 15210–15233 (2017).
14. S. E. Osborne, I. Matsumura, A. D. Ellington, Aptamers as therapeutic and diagnostic reagents: Problems and prospects. *Curr. Opin. Chem. Biol.* **1**, 5–9 (1997).
15. C.-H. Lu, X.-J. Qi, R. Orbach, H.-H. Yang, I. Mironi-Harpaz, D. Seliktar, I. Willner, Switchable catalytic acrylamide hydrogels cross-linked by hemin/G-quadruplexes. *Nano Lett.* **13**, 1298–1302 (2013).
16. J. Elbaz, Z.-G. Wang, R. Orbach, I. Willner, pH-stimulated concurrent mechanical activation of two DNA "Tweezers". A "SET-RESET" logic gate system. *Nano Lett.* **9**, 4510–4514 (2009).
17. C. Wang, M. P. O'Hagan, Z. Li, J. Zhang, X. Ma, H. Tian, I. Willner, Photoresponsive DNA materials and their applications. *Chem. Soc. Rev.* **51**, 720–760 (2022).
18. A. E. Rangel, A. A. Hariri, M. Eisenstein, H. T. Soh, Engineering aptamer switches for multifunctional stimulus-responsive nanosystems. *Adv. Mater.* **32**, 2003704 (2020).
19. J. Lloyd, C. H. Tran, K. Wadhwani, C. Cuba Samaniego, H. K. K. Subramanian, E. Franco, Dynamic control of aptamer-ligand activity using strand displacement reactions. *ACS Synth. Biol.* **7**, 30–37 (2018).
20. J. Elbaz, M. Moshe, I. Willner, Coherent activation of DNA tweezers: A "SET-RESET" logic system. *Angew. Chem. Int. Ed.* **48**, 3834–3837 (2009).
21. F. Wang, X. Liu, I. Willner, DNA switches: From principles to applications. *Angew. Chem. Int. Ed.* **54**, 1098–1129 (2015).
22. B. Yurke, A. J. Turberfield, A. P. Mills, F. C. Simmel, J. L. Neumann, A DNA-fuelled molecular machine made of DNA. *Nature* **406**, 605–608 (2000).
23. C. Teller, I. Willner, Functional nucleic acid nanostructures and DNA machines. *Curr. Opin. Biotechnol.* **21**, 376–391 (2010).
24. Y. Hu, F. Wang, C.-H. Lu, J. Girsh, E. Golub, I. Willner, Switchable enzyme/DNAzyme cascades by the reconfiguration of DNA nanostructures. *Chem.-Eur. J.* **20**, 16203–16209 (2014).
25. N. Wu, I. Willner, pH-stimulated reconfiguration and structural isomerization of origami dimer and trimer systems. *Nano Lett.* **16**, 6650–6655 (2016).
26. J. Wang, L. Yue, Z. Li, J. Zhang, H. Tian, I. Willner, Active generation of nanoholes in DNA origami scaffolds for programmed catalysis in nanocavities. *Nat. Commun.* **10**, 4963 (2019).
27. Z. Zhou, M. Vázquez-González, I. Willner, Stimuli-responsive metal-organic framework nanoparticles for controlled drug delivery and medical applications. *Chem. Soc. Rev.* **50**, 4541–4563 (2021).
28. W.-C. Liao, I. Willner, Synthesis and applications of stimuli-responsive DNA-based nano- and micro-sized capsules. *Adv. Funct. Mater.* **27**, 1702732 (2017).
29. D. Li, S. Song, C. Fan, Target-responsive structural switching for nucleic acid-based sensors. *Acc. Chem. Res.* **43**, 631–641 (2010).
30. Y. Weizmann, M. K. Beissenhirtz, Z. Cheglakov, R. Nowarski, M. Kotler, I. Willner, A virus spotlighted by an autonomous DNA machine. *Angew. Chem. Int. Ed.* **45**, 7384–7388 (2006).
31. Y. Hu, J. S. Kahn, W. Guo, F. Huang, M. Fadeev, D. Harries, I. Willner, Reversible modulation of DNA-based hydrogel shapes by internal stress interactions. *J. Am. Chem. Soc.* **138**, 16112–16119 (2016).
32. M. Vázquez-González, I. Willner, Stimuli-responsive biomolecule-based hydrogels and their applications. *Angew. Chem. Int. Ed.* **59**, 15342–15377 (2020).
33. J. S. Kahn, Y. Hu, I. Willner, Stimuli-responsive DNA-based hydrogels: From basic principles to applications. *Acc. Chem. Res.* **50**, 680–690 (2017).
34. L. Yue, S. Wang, Z. Zhou, I. Willner, Nucleic acid based constitutional dynamic networks: From basic principles to applications. *J. Am. Chem. Soc.* **142**, 21577–21594 (2020).
35. S. Wang, L. Yue, Z. Shpilt, A. Cecconello, J. S. Kahn, J.-M. Lehn, I. Willner, Controlling the catalytic functions of DNAzymes within constitutional dynamic networks of DNA nanostructures. *J. Am. Chem. Soc.* **139**, 9662–9671 (2017).
36. Z. Zhou, L. Yue, S. Wang, J.-M. Lehn, I. Willner, DNA-based multiconstituent dynamic networks: Hierarchical adaptive control over the composition and cooperative catalytic functions of the systems. *J. Am. Chem. Soc.* **140**, 12077–12089 (2018).
37. L. Yue, S. Wang, S. Lilienthal, V. Wulf, F. Remacle, R. D. Levine, I. Willner, Intercommunication of DNA-based constitutional dynamic networks. *J. Am. Chem. Soc.* **140**, 8721–8731 (2018).
38. L. Yue, S. Wang, V. Wulf, S. Lilienthal, F. Remacle, R. D. Levine, I. Willner, Consecutive feedback-driven constitutional dynamic networks. *Proc. Natl. Acad. Sci. U.S.A.* **116**, 2843–2848 (2019).
39. S. N. Semenov, A. S. Y. Wong, R. M. van der Made, S. G. J. Postma, J. Groen, H. W. H. van Roekel, T. F. A. de Greef, W. T. S. Huck, Rational design of functional and tunable oscillating enzymatic networks. *Nat. Chem.* **7**, 160–165 (2015).
40. K. Montagne, G. Gines, T. Fujii, Y. Rondelez, Boosting functionality of synthetic DNA circuits with tailored deactivation. *Nat. Commun.* **7**, 13474 (2016).
41. Z. Zhou, Y. Ouyang, J. Wang, I. Willner, Dissipative gated and cascaded DNA networks. *J. Am. Chem. Soc.* **143**, 5071–5079 (2021).
42. S. Wang, L. Yue, V. Wulf, S. Lilienthal, I. Willner, Dissipative constitutional dynamic networks for tunable transient responses and catalytic functions. *J. Am. Chem. Soc.* **142**, 17480–17488 (2020).
43. E. Del Grosso, E. Franco, L. J. Prins, F. Ricci, Dissipative DNA nanotechnology. *Nat. Chem.* **14**, 600–613 (2022).
44. Z. Li, J. Wang, I. Willner, Transient out-of-equilibrium nucleic acid-based dissipative networks and their applications. *Adv. Funct. Mater.* 2200799 (2022).
45. Y. Ouyang, P. Zhang, H. Manis-Levy, Y. Paltiel, I. Willner, Transient dissipative optical properties of aggregated Au nanoparticles, CdSe/ZnS quantum dots, and supramolecular nucleic acid-stabilized Ag nanoclusters. *J. Am. Chem. Soc.* **143**, 17622–17632 (2021).
46. J. Wang, Z. Li, Z. Zhou, Y. Ouyang, J. Zhang, X. Ma, H. Tian, I. Willner, DNAzyme- and light-induced dissipative and gated DNA networks. *Chem. Sci.* **12**, 11204–11212 (2021).
47. J. Kim, E. Winfree, Synthetic in vitro transcriptional oscillators. *Mol. Syst. Biol.* **7**, 465 (2011).
48. E. Franco, E. Friedrichs, J. Kim, R. Jungmann, R. Murray, E. Winfree, F. C. Simmel, Timing molecular motion and production with a synthetic transcriptional clock. *Proc. Natl. Acad. Sci. U.S.A.* **108**, E784–E793 (2011).
49. P. Subsoontorn, J. Kim, E. Winfree, Ensemble bayesian analysis of bistability in a synthetic transcriptional switch. *ACS Synth. Biol.* **1**, 299–316 (2012).
50. S. W. Schaffter, R. Schulman, Building in vitro transcriptional regulatory networks by successively integrating multiple functional circuit modules. *Nat. Chem.* **11**, 829–838 (2019).
51. K. Jiao, B. Zhu, L. Guo, H. Zhou, F. Wang, X. Zhang, J. Shi, Q. Li, L. Wang, J. Li, C. Fan, Programming switchable transcription of topologically constrained DNA. *J. Am. Chem. Soc.* **142**, 10739–10746 (2020).
52. S. Lilienthal, G.-F. Luo, S. Wang, L. Yue, A. Fischer, A. Ehrlich, Y. Nahmias, I. Willner, Constitutional dynamic networks-guided synthesis of programmed "genes," transcription of mRNAs, and translation of proteins. *J. Am. Chem. Soc.* **142**, 21460–21468 (2020).
53. S. Ohuchi, Y. Mori, Y. Nakamura, Evolution of an inhibitory RNA aptamer against T7 RNA polymerase. *FEBS Open Bio* **2**, 203–207 (2012).
54. A. Climent-Catala, T. E. Ouldridge, G.-B. V. Stan, W. Bae, Building an RNA-based toggle switch using inhibitory RNA aptamers. *ACS Synth. Biol.* **11**, 562–569 (2022).
55. C. Yan, P. J. Higgins, Drugging the undruggable: Transcription therapy for cancer. *Biochim. Biophys. Acta Rev. Cancer* **1835**, 76–85 (2013).
56. C. Toniatti, H. Bujard, R. Cortese, G. Ciliberto, Gene therapy progress and prospects: Transcription regulatory systems. *Gene Ther.* **11**, 649–657 (2004).
57. J. H. Bushweller, Targeting transcription factors in cancer—From undruggable to reality. *Nat. Rev. Cancer* **19**, 611–624 (2019).
58. A. J. Dzieciol, S. Mann, Designs for life: Protocell models in the laboratory. *Chem. Soc. Rev.* **41**, 79–85 (2012).
59. B. C. Buddingh', J. C. M. van Hest, Artificial cells: Synthetic compartments with life-like functionality and adaptivity. *Acc. Chem. Res.* **50**, 769–777 (2017).

Acknowledgments

Funding: This research was supported by the Israel Science Foundation (grant no. 2049/20) and by the Minerva Center for Complex Bio-hybrid Systems. **Author contributions:** Z.L. and J.W. formulated the systems, performed the experiments, analyzed the results, and participated in writing the paper. I.W. mentored the project, evaluated the results, and participated in writing the paper. **Competing interests:** The authors declare that they have no competing interests. **Data and materials availability:** All data needed to evaluate the conclusions in the paper are present in the paper and/or the Supplementary Materials.

Submitted 18 April 2022
Accepted 5 July 2022
Published 17 August 2022
10.1126/sciadv.abq5947